Numerical Simulation of Low-Grazing-Angle Ocean Microwave Backscatter and Its Relation to Sea Spikes

Charles L. Rino, *Fellow, IEEE*, and Hoc D. Ngo, *Member, IEEE*

***Abstract*—This paper presents the results of numerically simulating microwave backscatter from a deep-water breaking wave profile. Enhanced microwave backscatter from the crests of breaking waves has been hypothesized as the source of bright short-lived microwave radar echoes that are observed at low-grazing angles (LGA's). The characteristics of these "sea spikes" are distinctly different from the Bragg-scatter echoes that dominate measurements made at moderate grazing angles. Of particular interest is the high contrast that sea spikes present against ocean background backscatter when observed with horizontally polarized transmit/receive configurations [horizontal (HH) versus vertical (VV)]. This HH/VV contrast disparity has been attributed to polarization-selective cancellation of the direct reflection from the wave crest by the surface reflection. This hypothesis is reinforced first by showing evidence that VV polarization is suppressed in the intensity range that would normally be populated by the brightest scatterers. Histograms of unaveraged Doppler-centroid measurements show further that the depleted VV backscatter population is responding to scatterers that are moving much more slowly than the HH scatterers. The Doppler-centroid histograms provide a sharper delination between the two scattering populations than do the unconditionally averaged Doppler spectra that are more commonly reported. Finally, our numerical simulations show evidence of an interference mechanism that selectively suppresses VV backscatter. In our simulations, the polarization selectivity comes from the phase dependence of the backscatter from the wave crest. A Brewster phenomenon at the surface reflection point is not necessary.**

***Index Terms*—Sea surface electromagnetic scattering.**

I. Introduction

MODERN microwave radar and signal processing technology allows rapid real-aperture imaging of the ocean surface [1], [2]. Spatial resolution is constrained by the width of the antenna system L_e and the range of transmitted frequencies W. These parameters establish the azimuthal resolution ($\Delta\phi \sim \lambda/L_e$) and the range resolution ($\Delta r \sim 2c/W$) that can be achieved by applying beamforming and range-compression operations to the backscatter from an illuminated surface swath. It is convenient to represent the processed radar returns by a complex signal $v_{\phi_j}(r_m, t_n)$ referenced to the cell formed by the beam at $\phi_j = \phi_0 + (j-1)\Delta\phi$ and the range gate at $r_m = r_0 + (m-1)\Delta r$. Each resolution cell can be sampled at intervals $t_n = t_0 + (n-1)T$, where T is a multiple of the waveform repetition interval. Propagation delays and the sensitivity of the particular radar configuration ultimately limit the sampling rate $1/T$ for a fixed swath and number of beams. Irrespective of these details, however, the processed sample $v_{\phi_j}(r_m, t_n)$, which is indexed by beam, range gate, and time, is the most basic radar observable for remote sensing.

If the surface intercept occurs at grazing angle α, the backscatter represented by $v_{\phi_j}(r_m, t_n)$ is confined to an $r\Delta\phi$ by $\Delta r \cos\alpha$ resolution cell as long as the surface backscatter supports the necessary spatial coherence ($>L$), frequency coherence ($>W$), and temporal coherence ($>T$). What is observed also depends on nonlinear hydrodynamic processes that couple the unresolved ocean surface waves within the resolution cell to large-scale surface waves that pass through them. An important consequence is that the space-time evolution of the resolved waves can be captured by time-dependent Doppler spectra derived from the processed returns

$$\sigma(r_m, \delta_n; t_k) = \frac{T}{N}\left|\sum_{l=0}^{N} v(r_m, t_{l+kN}) \exp\{2\pi i \ln /N\}\right|^2 \tag{1}$$

where $\delta_n = n/(NT)$ with NT small compared to the orbital period of the resolved waves. The Doppler spread about the displaced centroid is a manifestation of the random motion of the unresolved scatterers, while the displacement of the Doppler centroid maps the evolution of the resolved waves. The temporally averaged RCS

$$\begin{aligned}\overline{\sigma}_T(r_m; t_k) &= \frac{1}{NT}\sum_{n=0}^{N} \sigma(r_m, \delta_n; t_k) \\ &= \frac{1}{N}\sum_{l=0}^{N} |v(r_m, t_{l+kN})|^2 \end{aligned} \tag{2}$$

captures a complementary range-time-intensity (RTI) image of the ocean surface.

While these purely phenomenological considerations can be used directly for radar remote sensing [2], [3], a quantitative relationship between the surface-height structure and the radar observable is necessary to fully exploit radar imaging of the ocean surface. To date, the theories that have been used to establish such relations remain restricted to gentle surface undulations. Bragg-scatter theory accommodates large-scale waves with embedded wavelength-scale components that are the primary source of the backscatter. The original two-scale theory developed by Valenzuela [4] captures the essential elements of this concept by varying the perturbation-theory

Manuscript received April 14, 1997; revised October 10, 1997. This work was supported in part by the Office of the Secretary of Defense under subcontract to Lawrence Livermore National Laboratory contract B160587 and by Vista Research, Inc. (internal funds).

The authors are with Vista Research, Inc., Mountain View, CA 94042 USA.

Publisher Item Identifier S 0018-926X(98)01041-2.

coordinates in response to surface tilts. There have been numerous variants of the two-scale theory, although developments that consistently combine large and small spatial components have just emerged [5]–[7]. To go beyond the limitations of the small-slope theories, however, it is necessary to revisit scatter theory at a fundamental level.

Surface backscatter is represented formally as the reradiation from source functions induced at the air-sea interface [8]. The source functions are determined by the incident electromagnetic field that illuminates the surface, the surface structure, and its electrical properties. At moderate grazing angles and small fractional bandwidths, the incident field remains confined by the compressed pulse. What results is a local relation between the radar observable and the surface structure. At low-grazing angles (LGA's), however, the surface area that can influence the source functions increases essentially without bound. Thus, LGA backscatter must accommodate both high curvature and an extended interaction region.

Because of the complexity of the problem, purely numerical methods provide the only viable means of testing the limitations imposed by approximations used in developing practical theories. The method of moments and iteration of the second-kind form of the surface-integral equations work well at moderate-grazing angles (see, for example, [9], [10] and references cited therein). However, to accommodate the large-surface realizations required for LGA computations, more efficient procedures are needed. Banded iterative matrix methods provided the first viable LGA simulations of surfaces well in excess of 100 wavelengths [11]. More recently, the forward–backward method developed by Holliday [12] and the method of ordered mutual interactions (MOMI) developed by Kapp and Brown [13] have provided alternative procedures that give insights into the physical scattering mechanism. Whereas most numerical simulations of rough-surface backscatter have emphasized average properties, the simulations by Milder and Smith cited above attack the dynamic evolution of nonlinear surfaces. This is an important step because it accommodates the spatially inhomogeneous and nonstationary (transient) structure of real ocean surfaces.

Pursuant to the phenomena that will be addressed in this paper, Lee *et al.* [14]–[16] have summarized the polarization- and grazing-angle-dependent backscatter characteristics of advancing waves as derived from Doppler-resolved X-band scatterometer data. By filtering average Doppler spectra from a translating sensor, Lee *et al.* identified vertically (VV)-dominant, comparatively short-lived "slow scatterers" and horizontally (HH)-dominant longer-lived "fast scatterers." The fast scatterers become more prominent with decreasing grazing angle. Because the water particles that define a breaking wave crest necessarily exceed the orbital acceleration of the linear-wave group that initiates the nonlinear evolution of the wave structure, the fact that fast scatterers are observed is not surprising. The challenge is to understand the mechanism that causes the anomalous scattering characteristics, particularly the fact that sea spikes are prominent only at LGA's.

In this paper, we first present some new results obtained from analysis of LGA microwave backscatter data from experiments conducted in western Scotland. In Rino *et al.* [3] a procedure we call epoch analysis is described. Briefly, Doppler analysis is performed using only the returns from range gates that are displaced systematically from the diagonal space–time RTI bands that delinate the sea spikes. By conditionally averaging the spectra from similarly displaced range gates, the dynamic evolution of structure can be measured in a reference frame moving with the apparent motion of the sea spikes. By applying this procedure, we showed that sea spikes from advancing waves are collocated with the fastest scatterers, which we identify with the wave crest. In receding waves, the weaker sea spikes are displaced down wave from the point of maximum Doppler shift. While the wave crests do not break uniformly, there is a high degree of statistical similarity in an ensemble of breaking wave structures. Evidently, a confluence of conditions is required to generate a sea spike.

In this paper, we present data analyses and numerical simulations that point to an interference mechanism as the source of the polarization-dependent contrast and Doppler disparity long associated with sea spikes. We present histograms of RCS measurements from single waveforms and histograms of Doppler centroids obtained from unaveraged pulse trains to support the interference hypothesis and the need for highly similar, but infrequently occurring conditions in space and time. The grazing-angle-dependent backscatter from a single deep-water breaking-wave profile as simulated by Wang *et al.* [17] is used to show that a sufficiently steepened breaking-wave structure can selectively reduce the VV-polarized backscatter from the tip of the wave via cancellation from the surface-reflected component. Because interference phenomena are known to be highly wavelength selective, the analysis is performed over a range of wavelengths as might be used in a high-resolution system.

Because small-slope theories with curvature corrections and numerical simulations can reproduce the grazing-angle dependence of the slow scatterers (see Voronovich [5, Fig. 6] and Rino and Ngo [18]), the new results presented here emphasize only the backscatter from the steepened crest of an otherwise smooth wave profile. Improved multiscale hydrodynamic simulations possibly can provide a complete numerical treatment [19], but insofar as we know, appropriately detailed hydrodynamic simulations have not yet been achieved.

II. LGA Backscatter

To guide the interpretation of the numerical simulations, we begin by reviewing LGA range-resolved backscatter data acquired with the Lawrence Livermore National Laboratory (LLNL) Hughes X-band radar operated from a hillside location at the Sound of Sleat, Scotland. The data were obtained as part of the joint U.S.–U.K. 1992 West Coast Scotland Experiment conducted at the Sound of Sleat, June 6–25, 1992. The radar transmits discrete frequencies centered near 10 GHz with alternating polarization and returns captured after each transmission to achieve high sensitivity, albeit at the expense of data rate. Data were recorded at a fixed grazing angle of 5.8° and processed by LLNL to extract calibrated HH and VV backscatter range-resolved to 2 m at a nearly 300-Hz sample

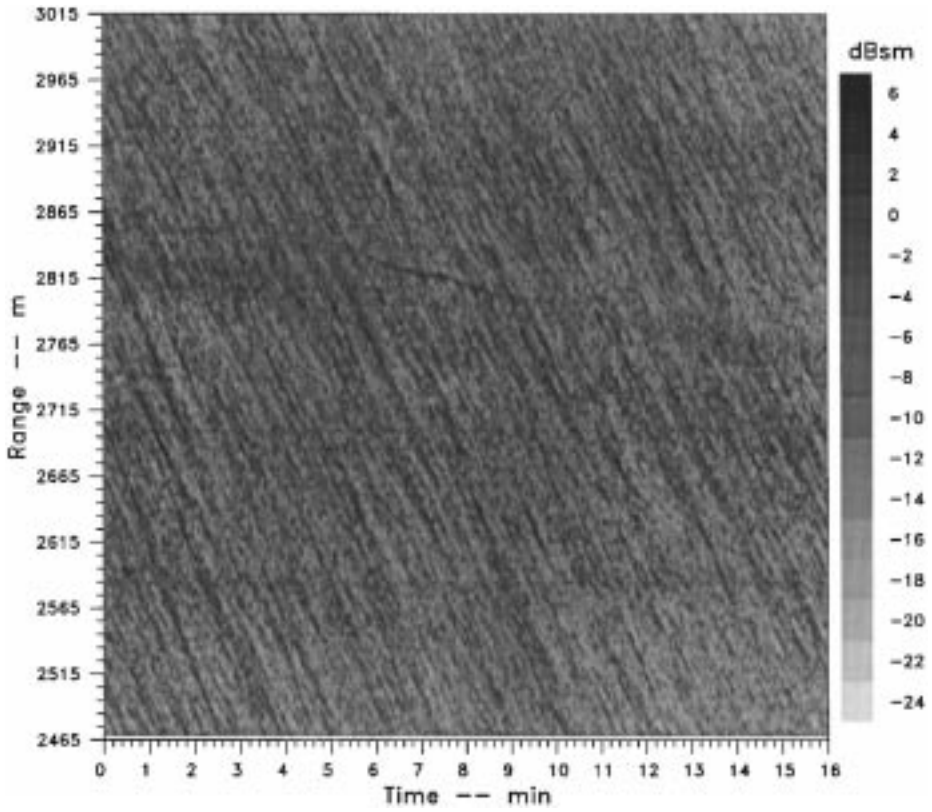

Fig. 1. RTI of HH up-wind, up-wave LGA backscatter from the western Scotland experiment.

rate. The 0.6° beam achieved 25-m azimuthal resolution at the central range of 2.5 km.

Figs. 1 and 2 show, respectively, RTI displays of HH and VV backscatter as defined by (2) with NT = 0.2 s. The strongest backscatter returns from both polarizations lie within coincident range-time bands with negative slopes corresponding to scattering centers advancing at ∼1.5 m/s. The predominant wind and wave motion was toward the radar. Although the brightest returns from each polarization are coincident in space and time, the HH returns have much higher contrast against their background with the largest peaks exceeding the corresponding VV returns by more than 10 dB. The average HH radar cross section (RCS) formed over the entire data frame (−8.5 dBsm) exceeds the corresponding VV RCS (−11.3 dBsm) average. There is much more that can be said about the surface dynamics as implied by the patterns of the resolved wave structure, but for our purposes, here we simply note that motion along the diagonal bands is at the group velocity of the linear-wave packet. This can be established by performing a dispersion analysis of intensity patterns and extracting the components that lie on the linear wave manifold [3], [20].

Ocean backscatter (clutter) is often characterized by the distribution of backscattered signal strength samples $|v_{\phi_0}(r_m, t_n)|^2$. From the clutter model developed by Jakeman and Pusey [21], one expects a Rayleigh distribution locally, which is modulated by the passage of wave crests through the beam. The modulation acts to form a composite distribution with an extended high RCS tail. The K, Weibull, and log-normal distribution all have this extended tail property. Fig. 3 shows single-waveform histograms, which have been normalized to unity maxima and plotted against the logarithm of RCS to emphasize the different shapes of the HH and VV distributions. The HH distribution behaves as the Jakeman–Pusey model predicts in that the log-RCS distribution is symmetric about its peak, which implies an enhanced probability of large RCS values. The general tendency of HH-polarized microwave backscatter from the ocean to form extended tail-like distributions at LGA's has been investigated by Trizna [22]. Trizna also noted the reduced high RCS tails for VV polarization prominent in the western Scotland data. For direct backscatter, we would expect the HH and VV histograms to be scaled versions of one another. While this is true for the scatterers that comprise the HH and VV returns that fall below their most probable values, the VV distribution appears to have a suppressed high RCS tail.

Before discussing this in more detail, we consider the Doppler characteristics. Fig. 4 shows typical near-simultaneous HH and VV Doppler spectra, as defined by (1). The HH centroid occurs at a higher Doppler shift (∼90 Hz) than does the corresponding VV centroid (∼40 Hz). Because the individual Doppler spectra are systematically shifted by the aforementioned nonlinear coupling to resolved surface waves, unconditioned averaging of high-resolution Doppler spectra smears the detail and makes the resultant average spectra difficult to interpret. Thus, we have calculated Doppler centroids after cyclically translating the spectra to provide a continuous function through the Nyquist frequencies

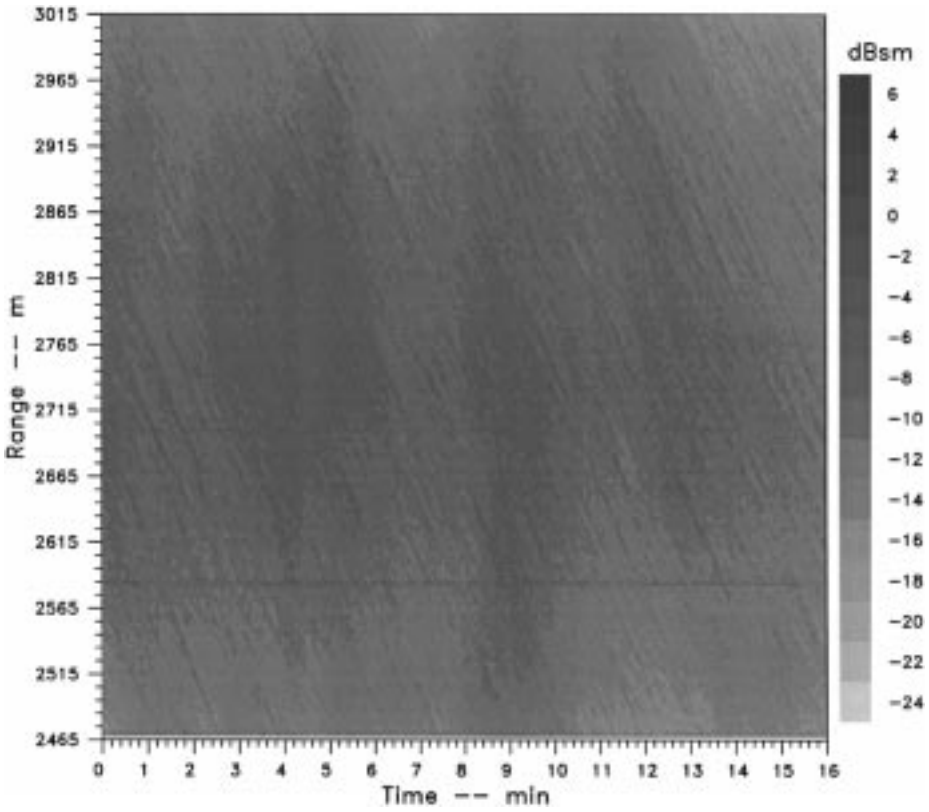

Fig. 2. RTI of VV up-wind up-wave LGA backscatter from western Scotland experiment.

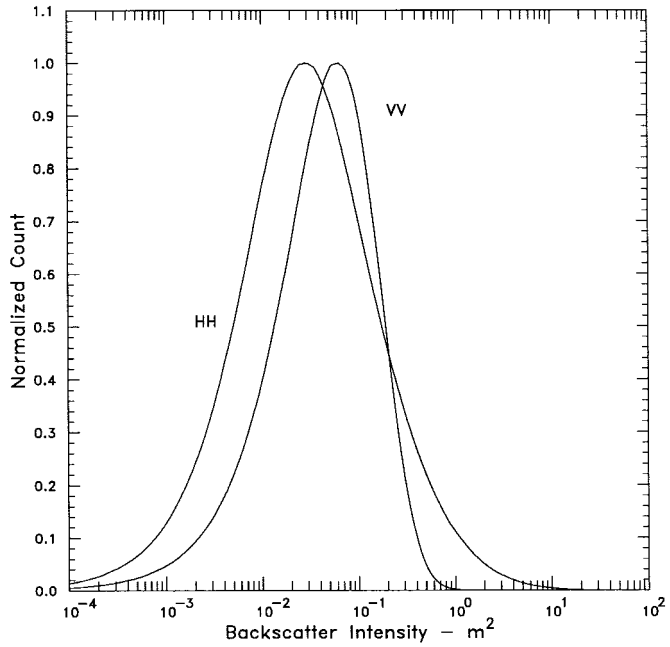

Fig. 3. Peak-normalized backscatter histograms from up-wind up-wave data shown in Figs. 1 and 2.

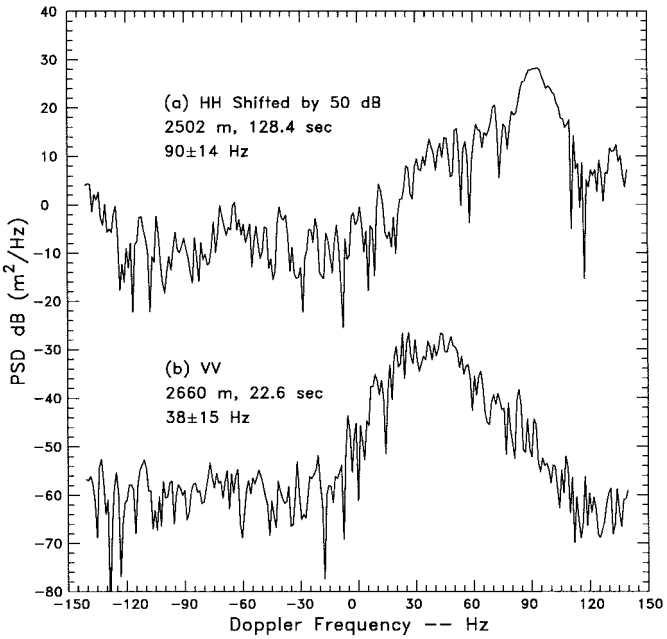

Fig. 4. Representative Doppler spectra obtained from single high RCS cell. Centroid frequencies are indicated.

near ±150 Hz. The centroids are local means calculated over the significant portion of the individual spectra. The Doppler centroids together with an estimate of their uncertainty are indicated on the Doppler spectra shown in Fig. 4.

Fig. 5 shows peak-normalized histograms of the Doppler centroids. The VV centroids accelerate abruptly to 40 Hz (0.6 mps) and then decay exponentially to fill a narrow Doppler range between 40–60 Hz, whereas the HH centroids show a broadened and more symmetric distribution about 85 Hz (1.3 mps). Evidently the VV backscatter is responding to slower scatterers confined to the back side of the wave while HH is responding to the fast scatterers near the wave crest. Because

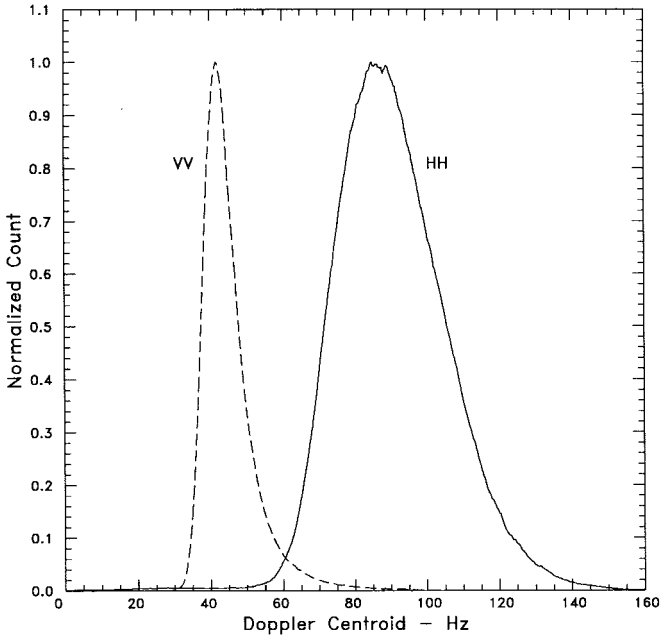

Fig. 5. Peak-normalized histograms of Doppler centroids from up-wind up-wave data.

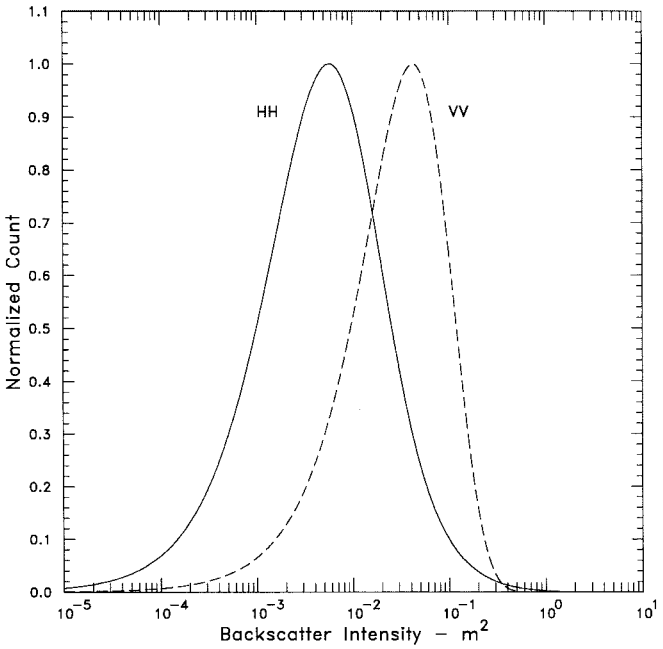

Fig. 6. Peak-normalized backscatter histograms from down-wind down-wave data.

the radar can localize structure only on a scale of a few meters, the Doppler centroids provide the most direct evidence of dual scattering populations.

If the slow scatterers are indeed Bragg-like structures distributed over the back side of the advancing wave, it is reasonable to invoke the angle dependence of Bragg-scattering as a mechanism that can suppress the contribution of the slow scatterers in HH backscatter, particularly in light of the small effective grazing angle. Thus, as Lee *et al.* have argued in the references cited in Section I, Bragg theory can explain the behavior of the slow scatterers qualitatively. Quantitative support has been provided by Voronovich [5]. It remains to demonstrate that the high curvature of the breaking wave crest is sufficient to account for the enhanced backscatter levels associated with the fast scatterers and to explain the HH-dominant scattering strength.

Although a breaking wave structure is highly asymmetric, we expect some mirroring of the backscatter characteristics when receding waves are illuminated. The RTI's from down-wind and down-wave western Scotland data show coincident banded structures, but with positive slopes indicative of scattering centers moving away from the radar. The main difference is an HH/VV intensity ratio closer to unity. Fig. 6 shows single-pulse histograms obtained under down-wind receding-wave conditions. Upon comparison with Fig. 3, we see that the respective HH and VV histograms have nearly identical shapes, but there is less separation between the most probable values. Fig. 7 shows the Doppler-centroid histograms for the receding wave backscatter. The distributions do indeed mirror the characteristics of their advancing-wave counterparts, although there is less separation between the peak centroid frequencies. The fact that HH polarization responds to slow scatterers when the backside of the wave faces the radar is qualitatively consistent with the Bragg theory because the illuminated backside is intercepted at a steeper local grazing angle. The polarization dependence of Bragg scatterers varies roughly as the fourth power of the secant of the incidence angle.

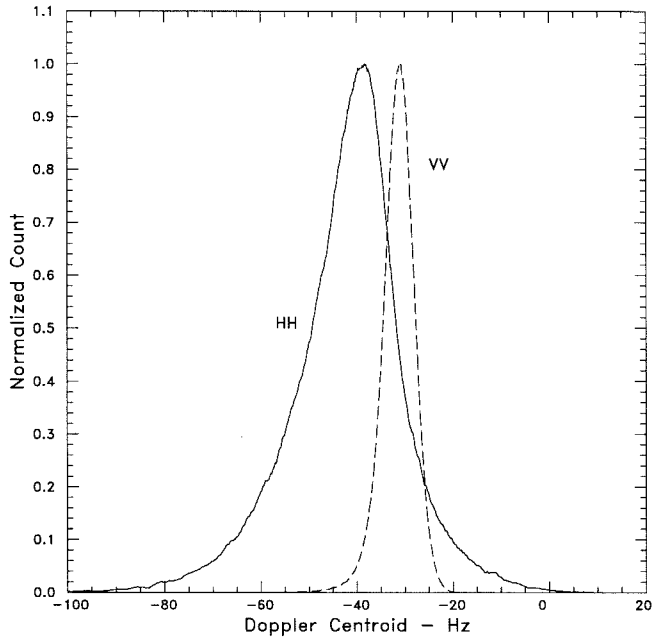

Fig. 7. Peak-normalized histograms of Doppler centroids from down-wind down-wave data.

To summarize, representative western Scotland data support the hypothesis that Bragg scatterers distributed over the gently sloped backside of a breaking wave can explain qualitatively the polarization-dependent characteristics of the slow LGA Doppler elements seen primarily with VV polarization. What

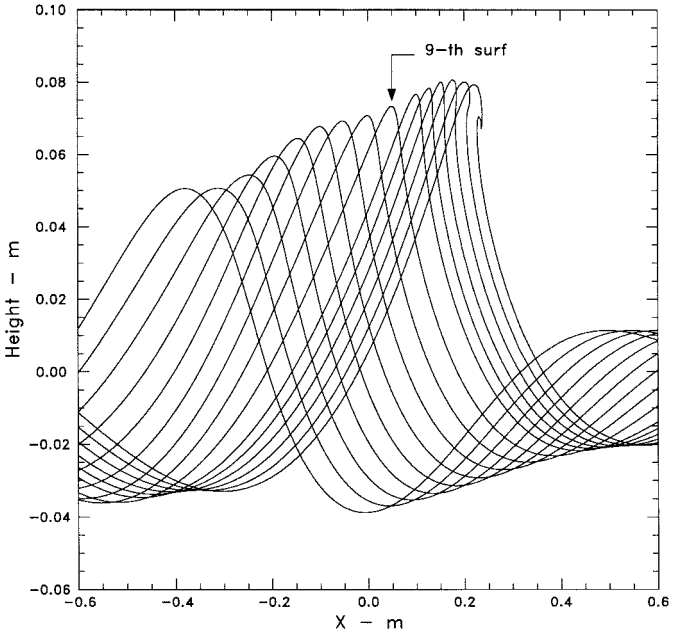

Fig. 8. Evolution of simulated deep-water breaking-wave profiles.

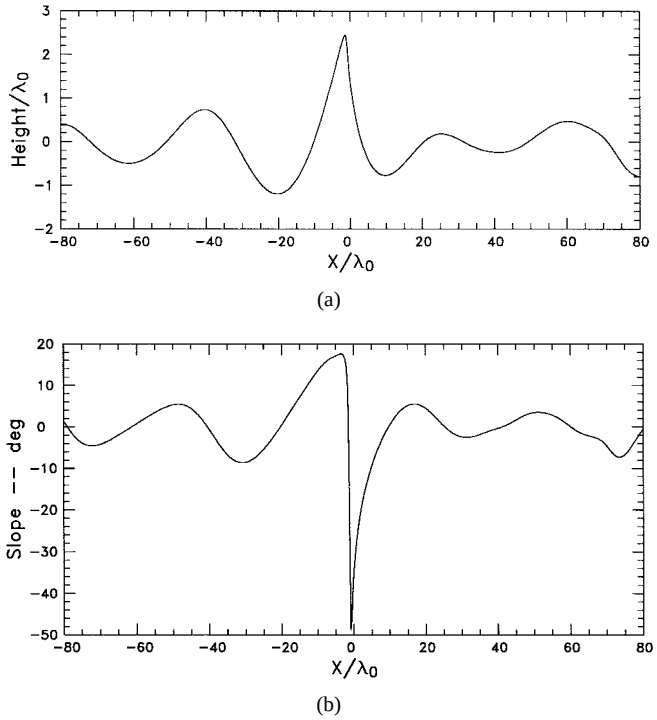

Fig. 9. Normalized surface height and average slope of central portion of surface profile nine used in backscatter simulations.

remains is to identify or demonstrate a possible mechanism that can account for the consistent suppression of the expected response of the stronger VV backscatter from the illuminated high-curvature crest of the breaking wave, whether it is viewed advancing where the cross section achieves its largest value or receding where the cross section is reduced. We will now show that the backscatter from a simulated deep-water breaking wave crest in the vicinity of a highly conducting surface displays such polarization-selective backscatter in the incipient phase of its breaking cycle. Sletten *et al.* [23], [24] have demonstrated similar results from wave tank measurements of breaking waves and from a model wave profile measured on a scattering range.

III. Numerical Simulations

Simulated breaking wave profiles were generated by the LONGTANK program developed by Wang *et al.* as described in [17]. A specific wave sequence has been used for cooperative studies by ourselves and others. Fig. 8 shows the sequence of profiles representing a wave group undergoing nonlinear steepening and subsequent overturning of the wave crest. Our results are from the ninth profile in the sequence. This profile was selected because it is sufficiently steepened to produce a prominent reflection, but has not yet overturned. The profile generates LGA backscatter levels at least 10 dB in excess of backscatter levels from Donelan Pierson surface realizations at the same grazing angles [5], [18]. The surface data points generated by LONGTANK were reinterpolated to 0.3-cm samples (10 per wavelength at 10 GHz), whereby 2004 uniformly spaced samples across the profile were retained. The profile was then zero-extended at both ends to generate 3000 surface-height samples for the numerical computations.

The extension of the surface is necessary for two reasons. First, we are looking for an interference effect between direct- and surface-reflected paths. An idealized planar surface is a good starting point to illustrate the phenomenon. The second reason is equally important, but commonly misunderstood. Grazing angle has meaning only relative to a horizontally extended structure. If, however, the structure that is being measured or simulated is not extended enough in wavelengths to resolve the grazing angle, the measurement or simulation becomes critically dependent upon the details of the illumination. The practical ramification of this fact is that in a real-world environment multiple-scattering effects can occur over significant distances at LGA's. For our purposes here, however, we want to demonstrate the interference phenomenon in its simplest form. The surface extension insures that we are observing only the interaction between the wave crest and the surface.

The resampled surface profile and its slope, the arc tangent of the derivative, are shown in Fig. 9. The surface height peaks at 2.5 wavelengths above the reference level and one wavelength below the reference level. The surface slopes range from 5° on the back side of the wave crest to -50° at its steepest point. There is no small-scale structure in the profile that would give rise to Bragg scatter. Thus, our analysis here addresses only the scatter that originates on the crest of the idealized deep-water breaking wave profile. The calculations were performed by using an exact point-matching method of moments (MoM) solution, although we have used a banded matrix inversion scheme nearly identical to that reported by Johnson *et al.* [11] to accommodate larger surface realizations. The incident field is a Gaussian beam, which is propagated consistently to the surface. The strong taper minimizes contamination from edge diffraction. The integrity

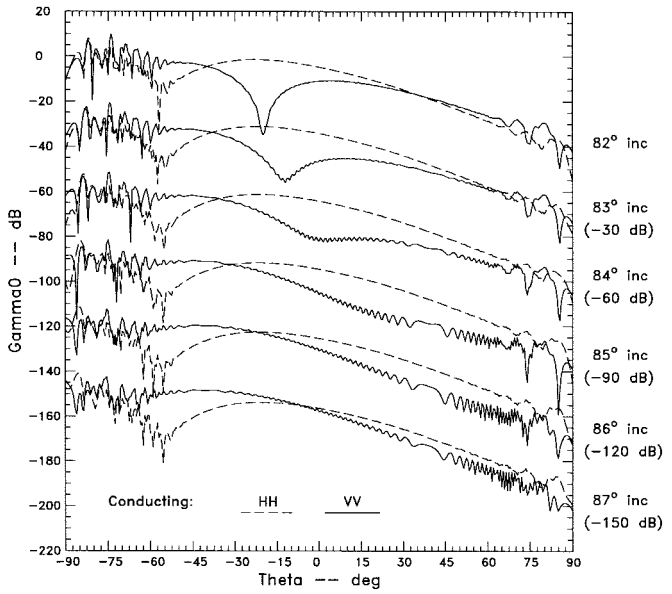

Fig. 10. Bistatic scatter profiles for incident illumination at incidence angles from 82° to 87° in 1° steps.

of the computation was checked by varying the sampling until energy was conserved to better than 10% at the largest incidence angle of 87°. Above 87° energy was conserved to better than 1%. Tests with different surface lengths verify that the results are independent of the incident beam shape within the resolved grazing angles supported by the surface extent. These consistency checks are described in more detail in Ngo and Rino [25]

Fig. 10 shows the HH- and VV-bistatic scatter for a perfectly conducting profile illuminated at incidence angles from 82° to 87° (8°–3° grazing). Near the backscatter direction, there is a progressive decrease in the VV-backscatter level relative to HH. Furthermore, the rapid variation of the VV-bistatic scatter with increasing grazing angle suggests an interference phenomenon. At 85° incidence, the VV backscatter is reduced nearly to zero, which is clearly a cancellation effect. To achieve complete cancellation, the wave crest must scatter isotropically and the surface must be 100% reflecting. The reciprocal surface reflections involving a single reflection can then interfere with the double-bounce surface path depending on the polarization-dependent phase imparted by the wave crest and the surface reflections. Near the pseudo Brewster angle for lossy dielectric surfaces ($\approx 6°$ at 10 GHz), the VV and HH reflections are oppositely phased; however, the backscatter from the wave crest also introduces a polarization-dependent phase change. Sletten *et al.* [24] emphasize the Brewster effect as manifest in the known behavior of an isotropic scatterer over a lossy dielectric surface.

However, the near-phase difference between HH- and VV-backscatter reflections is achieved, the resulting interference phenomena are highly sensitive to changes in frequency- and scattering-center height. Careful measurements and model comparisons could definitively resolve the source of the polarization-dependent phase mechanism and add support to the hypothesis. Toward this end, Fig. 11 shows the grazing angle and frequency dependencies of the HH/VV polarization ratio for the ninth profile. We see that the largest polarization ratios occur in narrow incidence-angle regions that vary systematically with frequency over a $\pm 20\%$ frequency change. Sletten *et al.* show similar behavior from laboratory measurements of an isotropic scatterer over ocean water. Systematic height variations of any structure that scatters uniformly toward the surface will produce a similar effect. The intermittence of the scatter within the diagonal bands in Figs. 1 and 2 can be attributed at least in part to such height variations. Ultrawide-band waveforms can be Fourier transformed to verify the frequency dependence of the polarization ratio. The pulse itself, however, would be elongated by the frequency dispersion. Thus, attempts to localize the scattering centers with wideband pulses may be futile.

IV. Discussion

In Section II of this paper, we summarized the characteristic of western Scotland LGA microwave backscatter data from advancing and receding waves by comparing histograms of the single-pulse backscatter strengths and the Doppler centroids. Interestingly, it was the HH-polarized backscatter that best fit the "standard" clutter model developed by Jakeman and Pusey. The HH distributions are nearly symmetric about their peak when plotted in log RCS units and merely shift in strength when observed from advancing and receding waves. By comparison, it is the VV distributions that are anomalous in being asymmetric about their peak values in log RCS units. Our interpretation of this observation is that the largest contributions were being suppressed. Histograms of the polarization-dependent Doppler centroids emphasize the most interesting attribute of LGA microwave backscatter, namely that HH backscatter responds mainly to the fastest scatterers whereas VV backscatter responds mainly to the slow scatterers.

These results support the conclusions of Lee *et al.* cited in Section I, namely that two types of scatterers are involved. Our results are also consistent with the hypothesis that Bragg scatterers distributed over the more gently sloped backside of a breaking wave can explain the look- and polarization-dependent characteristics of the slow scatterers. The look- and polarization-dependent characteristics of the fast scatterers can be explained by the interference mechanism demonstrated by Sletten *et al.* as well as by others cited in the references. The polarization dependence occurs because of the relative phase of the direct and surface-reflected paths. The Brewster effect from the conducting surface has been hypothesized as the source of the phase change. This mechanism is well-known in reflections from extended scatterers near dielectric surfaces. Our perfectly conducting results show, however, that the phase reversal can be induced by the high curvature unique to the breaking-wave structure. More detailed simulations and measurements could resolve the source.

It is beyond the scope of the current paper to present the results of pulse synthesis for both facing and receding profile illumination, although a complete treatment must address this

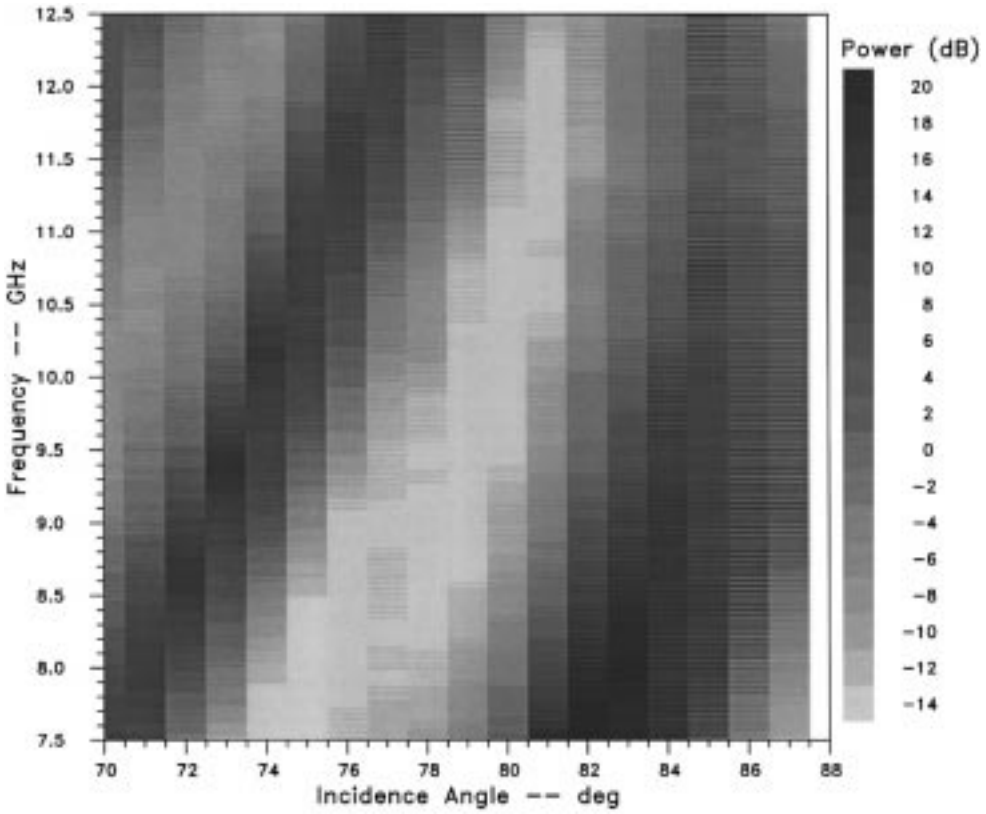

Fig. 11. Frequency and grazing angle dependence of HH/VV backscatter polarization ratio from surface profile nine.

aspect of the problem. Furthermore, two-dimensional wave profiles provide no information about variations along the crest itself. Without such variations, sea spikes would occur in uniform bands that progress at the phase velocity wave crest velocity. Apparent motion at the group velocity requires intermittence, which we suggest can be attributed to both the hydrodynamic evolution of the structure and its varying location relative to favorably aligned reflecting surfaces.

V. Conclusion

We conclude by addressing the question of why the fast scatterers are detected in microwave backscatter data recorded at moderate grazing angles. While the LGA cross-section enhancements of the wave crests are largest, the breaking-wave structure should still be detectable at moderate grazing angles, although the signature is competing with a stronger Bragg background. We suspect that conditional averaging relative to the resolved wave structure would betray the presence of fast scatterers. The fast scatterers are present, however, only on the crests of breaking waves. It is more difficult to isolate candidate features in backscatter data at moderate-grazing angles, but with modern computing resources it is feasible to organize large data sets and process them in this manner.

Acknowledgment

The authors would like to thank D. Holliday and L. DeRadd for their assistance in obtaining and processing the LONGTANK profiles.

References

[1] R. McIntosh, S. Frasier, and J. Mead, "FOPAIR: A focused phased array imaging radar for ocean remote sensing," *IEEE Trans. Geosci. Remote Sensing*, vol. 33, no. 1, pp. 115–124, Jan. 1995.

[2] R. McIntosh, S. Frasier, Y. Lin, D. Moller, and C. Lang, "Directional ocean wave measurements in a costal setting using a focused array imaging radar," *IEEE Trans. Geosci. Remote Sensing*, vol. 33, no. 2, pp. 428–440, Mar. 1995.

[3] C. L. Rino, E. G. Eckert, A. Siegel, T. Webster, A. Ochadlick, M. Rankin, and J. Davis, "X-band low-grazing-angle ocean backscatter obtained during LOGAN 1993," *J. Oceanic Eng.*, vol. 22, no. 1, pp. 18–26, 1997.

[4] G. R. Valenzuela, "Theories for the interaction of electromagnetic and ocean waves—A review," *Boundary Layer Meterol.*, vol. 13, pp. 61–85, 1978.

[5] A. G. Voronovich, "On the theory of electromagnetic waves scattering from the sea surface at low grazing angles," *Radio Sci.*, vol. 31, no. 6, pp. 1519–1530, 1996.

[6] D. M. Milder, "An improved formalism for electromagnetic scattering from a perfectly conducting rough surface," *Radio Sci.*, vol. 31, no. 6, pp. 1369–1376, 1996.

[7] R. A. Smith, "The operator expansion formalism for electromagnetic scattering from rough dielectric surfaces," *Radio Sci.*, vol. 31, no. 6, pp. 1377–1385, 1996.

[8] D. Holliday, "A radar ocean imaging model for small to moderate incidence angles," *Int. J. Remote Sensing*, vol. 7, no. 12, pp. 1809–1834, 1986.

[9] T. R. Michel and K. A. O'Donnell, "Angular correlation functions of amplitudes scattered from a one-dimensional, perfectly conducting rough surface," *J. Opt. Soc. Amer.*, vol. 9, pt. A, no. 8, pp. 1374–1384, 1992.

[10] T. R. Michel, M. E. Knotts, and K. A. O'Donnell, "Stokes matrix of a one-dimensional perfectly conducting rough surface," *J. Opt. Soc. Amer.*, vol. 9, pt. A, no. 4, pp. 585–596, 1992.

[11] J. T. Johnson, L. Tsang, R. T. Shin, K. Pak, C. H. Chang, A. Ishimaru, and Y. Kuga, "Backscattering enhancement of electromagnetic waves from two-dimensional perfectly conducting random rough surfaces: A comparison of Monte Carlo simulations with exterimental data," *IEEE Trans. Antennas Propagat.*, vol. 44, pp. 748–763, May 1996.

[12] D. Holliday, L. L. DeRaad, Jr., and G. J. St-Cyr, "Forward–backward: A new method for computing low-grazing angle scattering," *IEEE Trans. Antennas Propagat.*, vol. 44, pp. 722–729, May 1996.
[13] D. A. Kapp and G. S. Brown, "A new numerical method for rough-surface scattering calculations," *IEEE Trans. Antennas Propagat.*, vol. 44, pp. 711–721, May 1996.
[14] P. H. Y. Lee, J. D. Barter, K. L. Beach, C. L. Hindman, B. M. Lake, H. Rungaldier, J. C. Shelton, A. B. Williams, R. Yee, and H. C. Yuen, "X-band microwave backscattering from ocean waves," *J. Geophys. Res.*, vol. 100, no. C2, pp. 2591–2611, 1995.
[15] P. H. Y. Lee, J. D. Barter, K. L. Beach, E. Caponi, C. L. Hindman, B. M. Lake, H. Rungaldier, and J. C. Shelton, "Power spectral lineshapes of microwave radiation backscattered from sea surfaces at small grazing angles," *Proc. Inst. Elect. Eng. Radar, Sonar Navig.*, vol. 142, no. 5, pp. 252–258, Oct. 1995.
[16] P. H. Y. Lee, J. D. Barter, E. Caponi, M. Caponi, C. L. Hindman, B. M. Lake, and H. Rungaldier, "Wind-speed dependence of small-grazing-angle microwave backscatter from sea surfaces," *IEEE Trans. Antennas Propagat.*, vol. 44, pp. 333–340, Mar. 1996.
[17] P. Wang, Y. Yao, and M. P. Tulin, "Efficient numerical tank for nonlinear water waves based on the multi-subdomain approach with B. E. M.," *Int. J. Num. Math. Fluids*, vol. 20, pp. 1315–1336, 1995.
[18] C. L. Rino and H. D. Ngo, "The application of beam simulation to scattering at low grazing angles—Part II: Ocean-like surfaces," *Radio Sci.*, vol. 29, no. 6, pp. 1381–1391, 1994.
[19] D. G. Dommermuth, "Efficient simulation of short- and long-wave interactions with applications to capillary waves," *J. Fluids Eng.*, vol. 116, pp. 77–82, Mar. 1994.
[20] B. O. Werle, "Backscatter, spikes, and wave group observations at low grazing angles," in *Proc. IEEE Int. Radar Conf.*, 1995, pp. 187–195.
[21] E. Jakeman and P. N. Pusey, "A model for non-Rayleigh sea echo," *IEEE Trans. Antennas Propagat.*, vol. 24, no. 6, pp. 806–814, Nov. 1976.
[22] D. B. Trizna, "Statistics of low grazing angle radar sea scatter for moderate and fully developed ocean waves," *IEEE Trans. Antennas Propagat.*, vol. 39, pp. 1681–1690, Dec. 1991.
[23] M. A. Sletten and J. Wu, "Ultra-wideband, polarimetric radar studies of breaking waves at low grazing angles," *Radio Sci.*, vol. 31, no. 1, pp. 181–192, 1996.
[24] M. A. Sletten, D. B. Trizna, and J. P Hansen, "Ultra wideband radar observations of multipath propagation over the sea surface," *IEEE Trans. Antennas Propagat.*, vol. 44, pp. 646–651, May 1996.
[25] H. D. Ngo and C. L. Rino, "The application of beam simulation to scattering at low grazing angles, Part I: Methodology and validation," *Radio Sci.*, vol. 29, no. 6, pp. 1365–1379, 1994.

Charles L. Rino (S'62–M'70–SM'83–F'89), for photograph and biography, see p. 1347 of the September 1997 issue of this TRANSACTIONS.

Hoc D. Ngo (S'88–M'89), for photograph and biography, see p. 1347 of the September 1997 issue of this TRANSACTIONS.